Desalination and Water Treatment
www.deswater.com

doi: 10.1080/19443994.2015.1133323

57 (2016) 22551–22563
October

Taylor & Francis
Taylor & Francis Group

Synthesis of polyaniline/Fe_3O_4 magnetic nanoparticles for removal of reactive red 198 from textile waste water: kinetic, isotherm, and thermodynamic studies

Habib-Allah Tayebi[a,*], Zeinab Dalirandeh[b], Ali Shokuhi Rad[c], Ali Mirabi[b], Ehsan Binaeian[c]

[a]*Department of Textile Engineering, Qaemshahr Branch, Islamic Azad University, Qaemshahr, Iran, Tel. +98 1132322287; email: tayebi_h@yahoo.com*
[b]*Department of Chemistry, Qaemshahr Branch, Islamic Azad University, Qaemshahr, Iran, Tel. +98 2636557230; email: zeinab.dalirandeh@yahoo.com (Z. Dalirandeh), Tel. +98 9111284246; email: mirabi2012@yahoo.com (A. Mirabi)*
[c]*Department of Chemical Engineering, Qaemshahr Branch, Islamic Azad University, Qaemshahr, Iran, Tel. +98 9112134588; email: a.shokuhi@gmail.com (A. Shokuhi Rad), Tel. +98 1133209948; email: ehsan.binaeian@yahoo.com (E. Binaeian)*

Received 24 April 2015; Accepted 2 December 2015

ABSTRACT

In this study, polyaniline/Fe_3O_4 (PAni/Fe_3O_4) magnetic nanoparticles were synthesized and used as an adsorbent for the removal of Reactive Red 198 (RR 198) from water. Scanning electron microscope was used for determining morphology and size distribution of the prepared nanoparticles. The size of magnetic nanoparticles Fe_3O_4 was characterized by Transmission Electron Microscope. The formation of magnetic nanoparticles Fe_3O_4, was confirmed through X-ray Diffraction Technique. The chemical structures of the products were investigated with Fourier transform infrared spectroscopy. Effective parameters on the removal of RR 198 such as pH, dosage, and time were investigated and optimized. At the optimum situations the pH, dosage, and time were 5, 0.8 g l^{-1}, and 90 min, respectively. For determining the type of adsorption isotherm, Temkin, Langmuir, and Freundlich adsorption isotherms were used. The results revealed that Langmuir isotherm adequately met the experimental requirements. According to the Langmuir model, PAni/Fe_3O_4 magnetic nanoparticles sorbents exhibited the highest RR 198dye adsorption capacity of 45.454 mg g^{-1}. Kinetic analyses were conducted using pseudo-first and second-order models and the regression results showed that the adsorption kinetics was more accurately represented by the pseudo-second-order model. Thermodynamic parameters such as changes in Gibbs free energy (ΔG°), enthalpy (ΔH°), and entropy (ΔS°) were calculated. The negative values of ΔG° and the positive value of ΔH° (257.068KJ/mol) and ΔS° (104.590 J/mol K) show that the RR 198 adsorption on PAni/Fe_3O_4 magnetic nanoparticles was a spontaneous and endothermic process.

Keywords: Magnetic nanoparticles; Reactive dye; Adsorption; Isotherm; Kinetic study; Thermodynamic study

*Corresponding author.

1. Introduction

The pollution of natural waters induced by dyes and some noxious elements has recently been an important challenge for scientists in general [1]. These venomous and harmful materials are the cause of many serious problems in human and animals' body and plant tissues. In this case, the role of industrial factories and their chemical waste water is highlighted [2,3]. For instance, the effluence discharged from textile dyeing mills into the natural waters makes them inappropriate for public consumption [4]. Waste water from dyeing units in a textile plant often consists of highly concentrated dyes [5]. Dyes are used in various industries such as textiles, dyestuffs, cosmetics, paper, etc. [2,3]. Among all forms of dyes, azoic dyes which are complex aromatic structures resist highly to biodegradation [6]. Reactive red 198 is a water-soluble azo dye which is difficult to be removed from wastewater. There are several methods for removing dyes and other color contaminants: aerobic/anaerobic biological degradation, chemical coagulation, membrane filtration, flocculation, photochemical degradation, and chemical oxidation. These methods are not economical and none of them are able to totally remove dyes from waste water [7–10]. Among these methods, adsorption has now become popular because of its easy operations and low running costs [11,12]. Several adsorbents have been developed for the purification of wastewater including nano-scale zero valent iron, multi-walled carbon nanotube, micro crystalline naphthalene, SDS-coated Alumina, polyurethane foam, activated carbon, and conductive electroactive polymers such as polypyrrole and PAni [13–16]. PAni, as one of the most potentially useful conducting polymers, has recently received considerable attention, because of the low cost of its monomer [17–19]. PAni is a poly aromatic amine that can be easily synthesized chemically from Bronsted acidic aqueous solutions [17,19–22]. Chemical polymerization of aniline in aqueous acidic solutions can be performed using oxidizing agents such as KIO_3. Nanomaterials represent remarkable advantages due to their unique properties. In recent years, using magnetic nanoparticles in many fields, such as in protein separation [23–25], removal of metal ions and dyes [26–28], biotechnology, and biomedicine has had many pros because of their unique properties including the large surface area, small diffusion resistance [29–34], and easy separation of sorbent from sample solution by an external magnetic field [35]. In this study, PAni was synthesized directly on the surface of chemical route of Fe_3O_4 with magnetic nanoparticles at room temperature. Fe_3O_4 Magnetic nanoparticles coated with PAni was used as an adsorbent to remove RR 198 from aqueous solutions.

2. Method

2.1. Materials

All chemicals used in this study were analytical reagents grade and prepared in distilled water. Aniline was obtained from Merck and distilled before use. As shown in Fig. 1, PAni contains reduced (benzenoid diamine) and (1-y) oxidized repeat groups (quinoid diamine) and n is the degree of polymerization. HexadecylTrimethyl Ammonium Bromide (CTAB), ferrous chloride ($FeCl_2{\cdot}4H_2O$), ferric chloride ($FeCl_3{\cdot}6H_2O$), acetone, sulfuric acid, hydrochloric acid, and sodium hydroxide were used without further purification processes. Reactive red 198 (Reactive red RB),an anionic dye, was purchased from Dystar (see Fig. 2 and Table 1), and was used as received without further purification. A stock solution of Reactive red RB (1,000 mg L^{-1}) was prepared and suitably diluted to the required initial concentration. This dye shows an intense absorption peak in the visible region at 515 nm (Fig. 3). This wavelength corresponds to the maximum absorption peak of the RR 198 (λ_{max} = 515). Calibration curve of absorbance against Reactive red RB concentration was obtained using standard Reactive red RB solutions at pH 5. The calibration curve shows that Beer's law ($A = \varepsilon bc$) is obeyed in concentration range (0.01–100 mg L^{-1}). The experimental data reported in Fig. 4 were fitted by a straight line with a high regression coefficient value (r^2 = 0.999). The pH adjustments were carried out using diluted NaOH (1.0 mol L^{-1}) and HCl (1.0 mol L^{-1}) solutions. A UV–vis spectrophotometer (Jenway model 6505) with a 1 cm cell was used to measure absorption data. pH measurements were made with a Metrohm model 744 pH meter with a combined pH glass electrode calibrated against two standard buffer solutions at pH 4.0 and 7.0. The surface morphology of the powders was observed by the scanning electronic microscope (SEM, LEO 440i, Leo Electron Microscopy, Cambridge, England). The size of magnetic nanoparticles Fe_3O_4 was characterized by Transmission Electron Microscopy (TEM, Hitachi, HF2000, Hitachi High-Technologies Europe GmbH, Krefeld, Germany). The products of chemical structures were investigated with Fourier transform

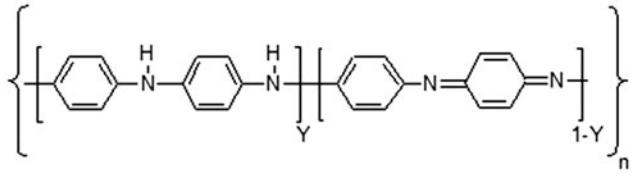

Fig. 1. Structure of PAni in various oxidation states.

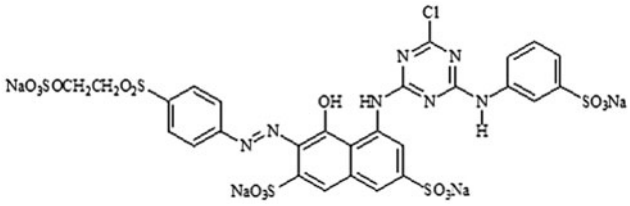

Fig. 2. Chemical structure of RR 198.

infrared spectroscope (FTIR Shimadzu model 4100, Japan). Fe_3O_4 magnetic nanoparticles (MNPs) were examined by X-ray diffraction (XRD, Japan Jeol JDX-8030 operated at 30 kV and 20 mA). An electronic analytical balance (cp 153 sartorius) was used for weighing the solid materials. Other instruments were hand-made stirrer, magnet (with 1.4 T magnetic strength) and an ultrasonic bath EUROSONIC4D.

2.2. Preparation of nanosize Fe_3O_4

Fe_3O_4 MNPs were prepared through chemical co-precipitation method. First, to prepare a stock solution of ferrous and ferric ions, 5.2 g $FeCl_3{\cdot}6H_2O$, 2.0 g $FeCl_2{\cdot}4H_2O$ and 0.85 mL HCl (12 mol L^{-1}) were dissolved in 25 mL distilled water in a beaker which was degassed with nitrogen gas for 20 min before use. On the other hand, 250 mL of 1.5 mol L^{-1} NaOH solution was degassed (for 15 min) and heated up to 80°C in the reactor. Then, it was added dropwise into the stock solution using a dropping funnel during 30 min under nitrogen gas protection and was stirred by a hand-made stirrer. During the whole process, the solution temperature remained at 80°C and nitrogen gas was used to prevent the intrusion of oxygen. After the reaction, the obtained Fe_3O_4 MNPs were separated from the reaction medium by magnetic field (with 1.4 T magnetic strength), and rinsed with 250 mL distilled water and then, the product was oven dried at 90°C.

2.3. Preparation of PAni/Fe_3O_4 nano composite

One gram of KIO_3 was added to 100 mL sulfuric acid (1 M) and then a uniform solution was resulted using magnetic mixer. After 10 min, 1 g MNPs and 0.2 g CTAB were added to the solution and after 20 min, 1 mL fresh distilled aniline monomer was added to the stirred solution. The reaction was carried out for 5 h at room temperature. PAni/Fe_3O_4 nano composite particles were separated from the reaction media by placing a strong magnet, and rinsed several times with deionized water and acetone, and dried at 60°C temperature in an oven for 24 h and stored in a desiccator for subsequent use.

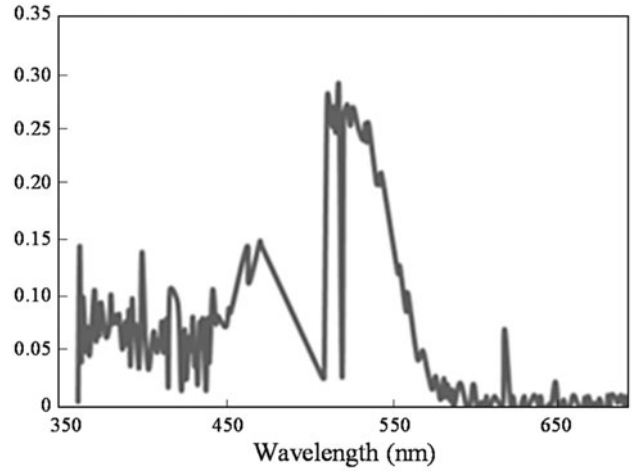

Fig. 3. Vis spectrum obtained for RR 198 in distilled water.

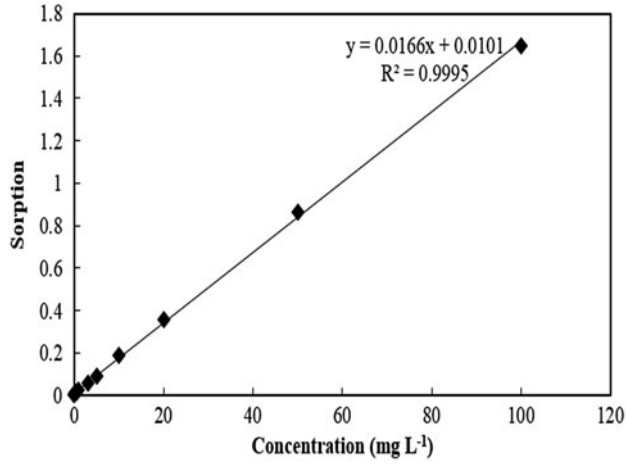

Fig. 4. Calibration curve of absorbance against concentration of RR 198.

Table 1
Characteristics of RR 198

Name	CAS number	C.I. number	Formula	Molecular weight	λ_{max}
Reactive red 198	145,017-98-7	18,221	$C_{27}H_{18}ClN_7Na_4O_{15}S_5$	968.21 g/mol	515

2.4. Adsorption of RR 198

Adsorption studies were performed by adding 0.07 g nano composite to the 100 mL of RR 198 solution (20 mg L^{-1}) in a beaker. The pH value of the RR 198 solution was adjusted to 5 using HCl0.1 M and NaOH0.1 M and the solution was shaken by a mechanical stirrer for 90 min. Subsequently, the magnetic adsorbent was isolated easily and quickly by magnetic field and the aqueous solution was centrifuged at 4,000 rpm for 20 min. The concentration of RR 198 in the solution was measured spectrophotometrically at 515 nm.

3. Result and discussion

3.1. Surface morphology

A scanning electron microscopy (SEM) image of MNPs-Fe_3O_4 before and after coating with PAni is illustrated in Fig. 5(a) and (b), respectively. The coating with the polymer produced by the surface polymerization is clearly visible. The coating of MNPs has been found to be uniform by visual inspection.

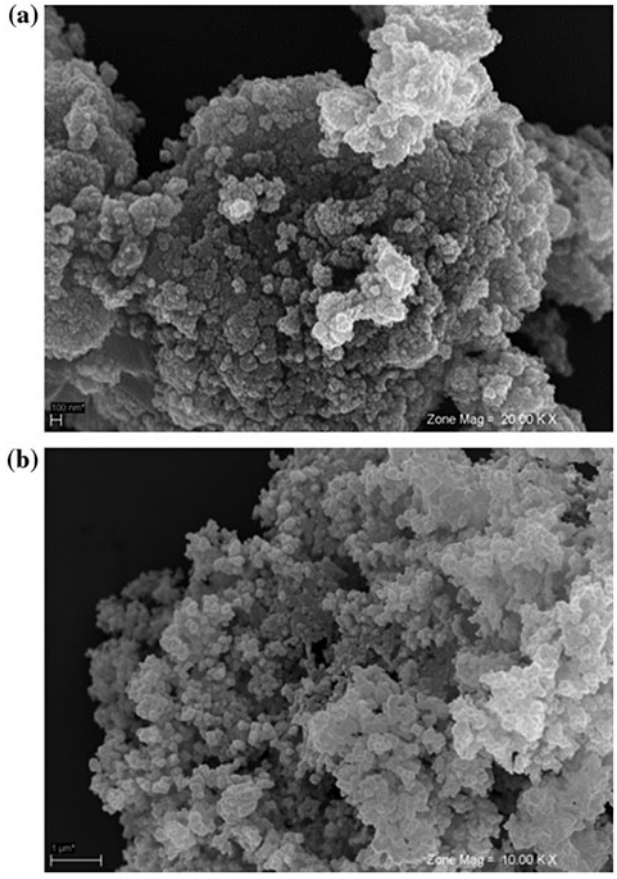

Fig. 5. (a) SEM image of Fe_3O_4 nanoparticles before coating with PAni and (b) SEM image of Fe_3O_4 nanoparticles after coating with PAni.

3.2. Structural characterization

The TEM image showed that most of the MNPs were less than 50 nm in diameter, as indicated in Fig. 6. The identity and purity of the MNPs–Fe_3O_4 were verified by XRD (Fig. 7) [36,37].

The structure of the obtained product was determined by FTIR spectrum. The FTIR spectroscopy provided important information regarding the formation of PAni/Fe_3O_4 nano composite. FTIR analysis was done to identify the characteristic peaks of the product. FTIR spectra for PAni, Fe_3O_4 MNPs, and PAni/Fe_3O_4 nano composite are shown in Fig. 8(a), (b) and (c), respectively. As can be seen, PAni shows the presence of the characteristic absorption bands at 1,559.18 cm^{-1} (C=C stretching vibration of the quinoid ring), 1,486 cm^{-1} (stretching vibration of C=C of the benzenoid ring), 1,304 cm^{-1} (C–N stretching vibration), 1,130 cm^{-1} (C–H in-plane deformation), and 811 cm^{-1} (C–H out of- plane deformation). It can be seen that the characteristic peak of magnetic Fe_3O_4 appeared at 584.3 cm^{-1} [38].

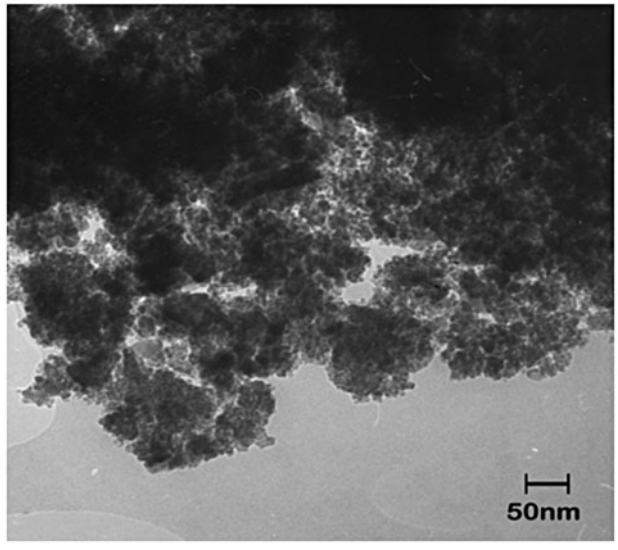

Fig. 6. TEM image of Fe_3O_4 nanoparticles.

3.3. Effect of pH

The pH value of the aqueous solution is an important controlling parameter in the adsorption process. These pH values influence the surface charge of adsorbent during adsorption. In order to assess the

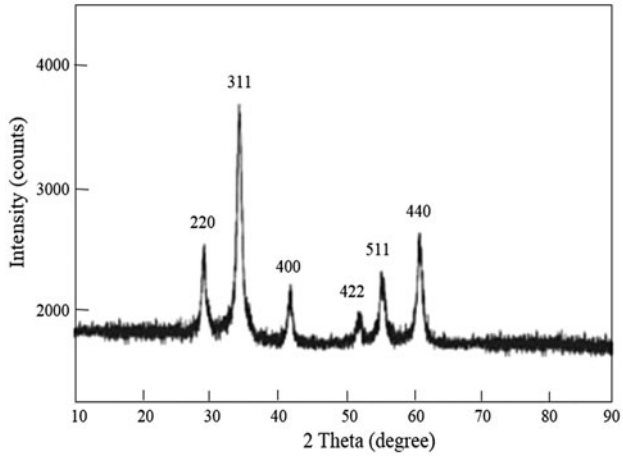

Fig. 7. XRD pattern of Fe_3O_4 nanoparticles.

influence of this parameter on the adsorption, the experiments were carried out at different initial pH ranging from 2 to 12. The experiment was performed on PAni and PAni/Fe_3O_4 nano composite with an initial concentration of 20 mg/L at room temperature with contact time of 90 min. The results are shown in Fig. 9. Removal of RR 198 increased with decreasing pH and a maximum value was reached at an equilibrium pH of around 5 (see Fig. 9). This happened because in acidic environments, the amino groups of Polymer PAni ($–NH_2$) are protonated in the presence of the released H^+ Protons in the environment; therefore, the adsorption of RR 198, which has a negative charge, increases. With protonation of the adsorption surface, the tendency of RR198 to the adsorption surface increases. In comparison with the adsorption of PAni, PAni composite adsorbs more dye because of the tiny size of the magnetic nanoparticles of iron oxide (about 50 nm). With the placement of polymer nanoparticles of PAni on the composite, more amino groups of PAni were available. Thus, more dye was adsorbed on the composite.

3.4. Influence of sorbent dosage

The removal percentage of RR 198 was measured by varying the adsorbent (PAni and PAni/Fe_3O_4) dose between 0.01 and 0.1 g at dye concentration of 20 mg/L. The results are presented in Fig. 10. On increasing the adsorbent dose to 0.08 g, the amount of dye sorption increased as the adsorbing sites on the adsorbents increased. However, the increase in the adsorbent dose to more than 0.08 g did not cause any increase in sorption, so the amount of sorption remained constant because of the accumulation of the adsorbents. In comparison with the adsorption of PAni, PAni composite adsorbs more dye because of the tiny size of the magnetic nanoparticles of iron oxide (about 50 nm). With the placement of polymer nanoparticles of PAni on the composite, more amino groups of PAni were available, so

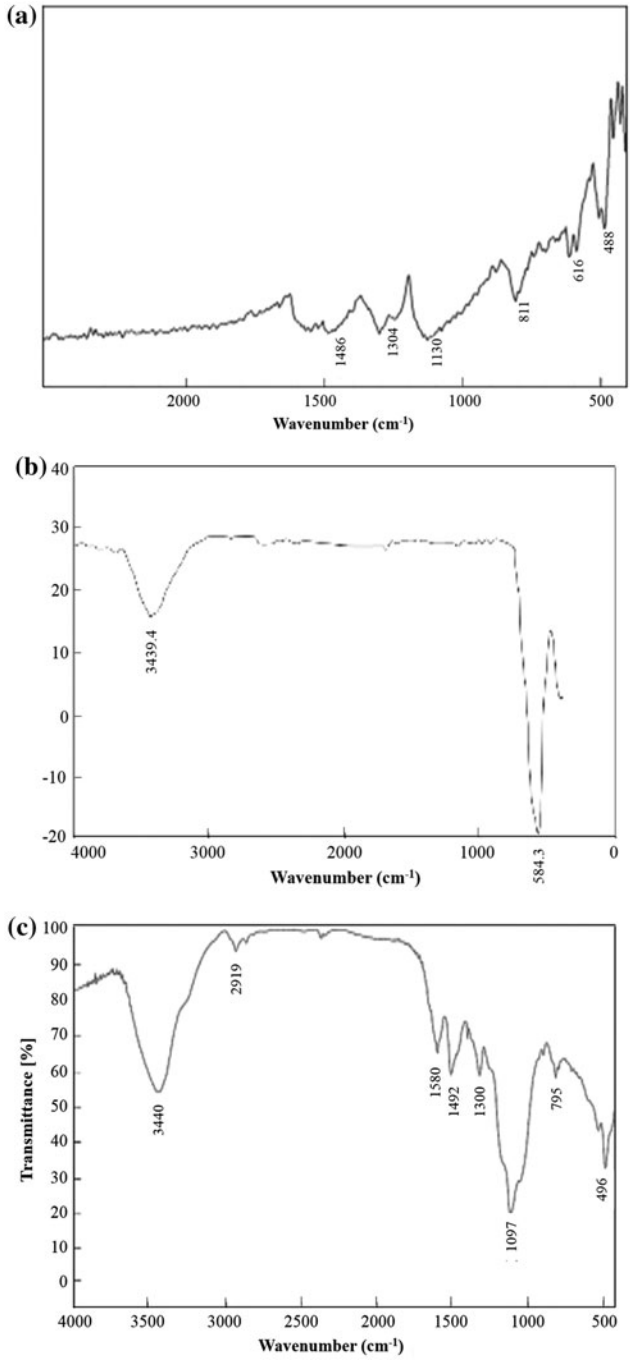

Fig. 8. (a) FTIR spectra of PAni, (b) FTIR spectra of MNPs-Fe_3O_4 and (c) FTIR spectra of PAni/Fe_3O_4 nano composite.

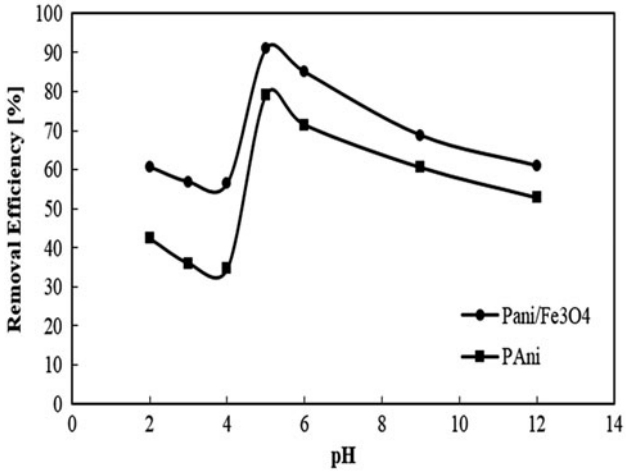

Fig. 9. Effect of pH on the removal efficiency with: PAni/Fe_3O_4 and PAni (the initial concentration, contact time, volume of solution and amount of adsorbent was 20 mg/L, 90 min, 100 mL and 0.07 g, respectively).

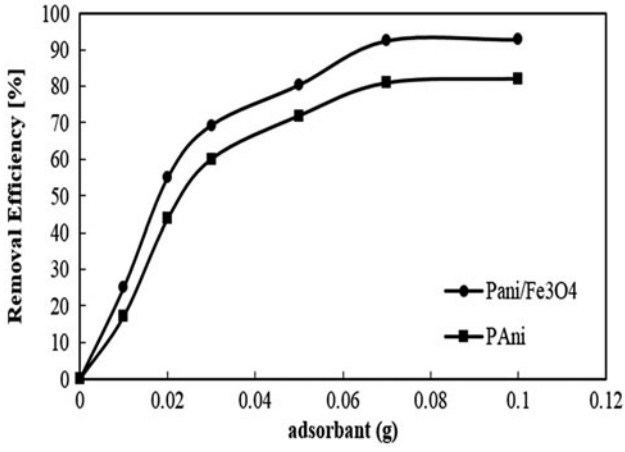

Fig. 10. Effect of adsorbent dosage on the removal efficiency with: PAni/Fe_3O_4 and PAni (the initial concentration, pH, contact time and volume of solution was 20 mg/L, 5, 90 min and 100 mL, respectively).

more dye was adsorbed on the composite. This finding was also obtained through investigating the effect of pH.

The RR 198 removal efficiency increases up to an optimum dosage beyond which the removal efficiency does not change significantly. This result was anticipated because for a fixed initial solute concentration, increasing adsorbent doses provides greater surface area and more adsorption sites, whereas the adsorbed RR 198 quantity per unit weight of the sorbent decreased by increasing the magnetic beads quantity. At the very low adsorbent concentration, the absorbent surfaces became saturated with the dye and the residual dye concentration in the solution was high.

3.5. Effect of contact time and temperature

Fig. 11 shows the effect of contact time and temperature on sorption of RR 198 by PAni/Fe_3O_4. In this regard, initial dye concentration of 70 mg/L, pH of 5, and PAni/Fe_3O_4 dose of 0.1 g in 100 mL were used. The mixture was agitated in a mechanical shaker for different periods of contact time (5–180 min) and different temperatures) 25, 35, and 45˚C). The obtained results are summarized in Fig. 11. These results revealed that the adsorption of RR 198 was fast at first (until 60 min) and the equilibrium was achieved after 90 min of contact time. Taking into account these results, a contact time of 90 min was chosen for further experiments and it was also observed that the removal efficiency increases with the increase in solution temperature because the dye molecules mobility increases with increasing temperature. Therefore, a number of molecules obtain enough energy to undergo an increasing interaction with active sites at sorbent surface. These findings reveal that RR 198 adsorption on PAni composite is endothermic.

3.6. Adsorption isotherms

Appropriate correlations in the equilibrium data have fundamental importance in the design of an adsorption system for removing dyes. In the present study, three isotherm models have been tested for treatments of the equilibrium adsorption data.

3.6.1. Langmuir isotherm model

Langmuir theory was based on the assumption that the uptake of adsorbate occurs on a homogeneous

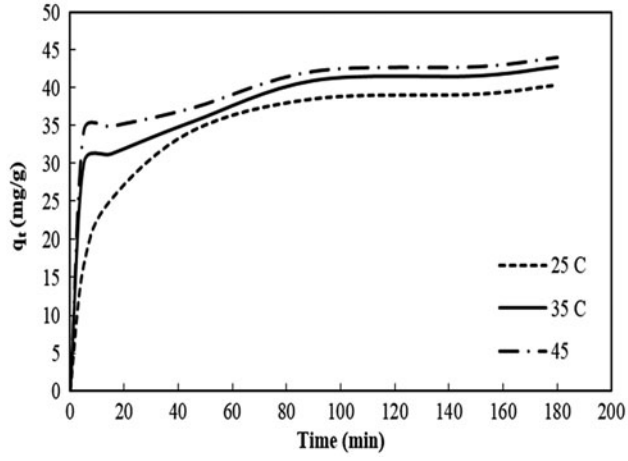

Fig. 11. Effect of contact time and temperature on the removal efficiency with: PAni/Fe_3O_4 (the initial concentration, pH, volume of solution and amount of adsorbent was 70 mg/L, 5, 100 mL, and 0.1 g, respectively).

surface by monolayer adsorption and adsorption energy is constant in this model. The theory can be represented by the following equations:

$$q_e = \frac{q_m k_L C_e}{1 + k_L C_e} \quad (1)$$

where q_e is the quantity of dye adsorbed (mg/g) at equilibrium, C_e is the equilibrium dye concentrations in residual dyeing bath (mg/L), and k_L (L/mg) and q_m (mg/g) are the Langmuir constants.

Table 2 shows that the Langmuir isotherm model could be linearized to at least four different types [39]. The Langmuir constants k_L, and q_m values can be calculated from the plot between C_e/q_e vs. C_e, $1/q_e$ vs. $1/C_e$, q_e vs. q_e/C_e, and q_e/C_e vs. q_e for type 1, type 2, type 3, and type 4 Langmuir isotherms, respectively.

Table 3 shows the predicted isotherm constants (k_L and q_m) and the corresponding R^2 values. The isotherm parameters obtained from the four linearized Langmuir isotherms were different. Type 1 Langmuir isotherm (Fig. 12) was found to be the best fitting linearized Langmuir expression with coefficient of determination of approximately 1. Therefore, the results were taken from Langmuir equation type 1. Correlation coefficients are near to 1 which means that experimental data fitted in this model well.

Essential characteristics of the Langmuir-type adsorption process can be classified by a term "R_L," a dimensionless constant separation factor. The R_L value indicates the favorability and the shape of the isotherms as follows:

$$R_L = \frac{1}{1 + K_L C_0} \quad (2)$$

R_L is a dimensionless constant separation factor, C_0 is the initial concentration of dye solution (mg/L), and k_L is the Langmuir constant (L/mg), the parameter R_L indicates the shape of the isotherm accordingly. Table 3 depicts the values of R_L. The magnitude of the exponent R_L gives an indication of the favorability of adsorption. According to Table 4, Values of $0 < R_L < 1$ represent favorable adsorption conditions.

3.6.2. Freundlich isotherm model

The Freundlich isotherm model equation deals with physicochemical adsorption on heterogeneous surface at sites with different energy of adsorption and with non-identical adsorption sites that are not always available [40]. Mathematically, it is characterized by the heterogeneity factor "$1/n$":

$$q_e = k_F C_e^{1/n} \quad (3)$$

where K_F is the Freundlich constant and n is the heterogeneity factor. The K_F value is related to the adsorption capacity, while $1/n$ value is related to the adsorption intensity. Freundlich model can be represented by the linear form as follows:

$$\ln q_e = \ln k_F + 1/n \ln C_e \quad (4)$$

Therefore, K_F and $1/n$ can be determined from the linear plot of $\ln q_e$ against $\ln C_e$. The K_F and n values are listed in Table 5. Correlation coefficient is below 0.95 suggesting that experimental data is not fitted to this model. The value of correlation coefficient is lower than the other three isotherms values. The Freundlich isotherm (Fig. 13) represents the poorer fit of experimental data than the other isotherms.

3.6.3. Temkin isotherm model

Temkin isotherm is based on the assumption that the decrease in the heat of adsorption of all the molecules in layer is linear and the adsorption is characterized by a uniform distribution of binding energies. Temkin model can be represented by the linear form as follows:

$$\ln(C_e) + K_1 \ln(K_2) q_e = K_1 \quad (5)$$

Table 2
Langmuir isotherm and its linear forms

Langmuir isotherm		Linear form	Plot
Type 1	$q_e = \frac{q_m k_L C_e}{1 + k_L C_e}$	$\frac{C_e}{q_e} = \frac{1}{q_m} C_e + \frac{1}{k_L q_m}$	C_e/q_e vs. C_e
Type 2		$\frac{1}{q_e} = \frac{1}{k_L q_m C_e} + \frac{1}{k_L q_m}$	$1/q_e$ vs. $1/C_e$
Type 3		$q_{e=} q_m - \frac{q_e}{k_L C_e}$	q_e vs. q_e/C_e
Type 4		$\frac{q_e}{C_e} = k_L q_m - k_L q_e$	q_e/C_e vs. q_e

Table 3
Calculated Langmuir isotherm parameters by different linear method

Langmuir adsorption isotherm	Type 1	Type 2	Type 3	Type 4
q_m	45.454	52.631	48.57	50.240
K_L	0.128	0.070	0.083	0.075
R^2	0.995	0.974	0.904	0.904
R_L	0.072	0.125	0.107	0.117

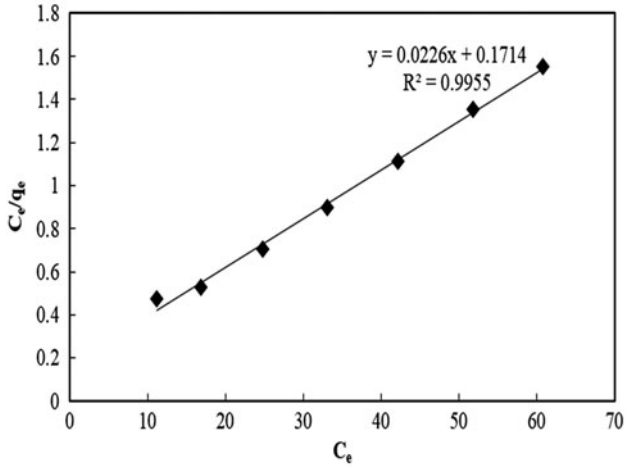

Fig. 12. Removal of dye RR198 with: PAni/Fe_3O_4 (the initial concentration, pH, volume of solution and amount of adsorbent was 70 mg/L, 5, 100 mL, and 0.1 g, respectively), Type 1 Langmuir isotherm.

Table 4
Values of separation factor R_L

Value of R_L	Type of isotherm
$R_L > 1$	Unfavorable
$R_L = 1$	Linier
$R_L = 0$	Irreversible
$0 < R_L < 1$	Favorable

where K_2 is the equilibrium binding constant, corresponding to the maximum binding energy, and constant K_1 is related to the heat of adsorption. K_1 and K_2 can be determined from the linear plot of ln q_e against ln C_e (see Fig. 14). The K_1 and K_2 values are listed in Table 5. Correlation coefficient is below 0.95 suggesting that experimental data is not fitted to this model. The fitting of the data, obtained from the sorption of RR 198 on PAni/Fe_3O_4, to the three isotherm models showed that the linearity of the Langmuir isotherm type 1 model ($r^2 = 0.9955$) was higher than that of the other isotherm models (Table 5).

It shows that the sorption of RR 198 on PAni composite was one layered and took place in specific spots of homogeneous protonated amino groups on the sorption surface of the Polymer PAni in the acidic environments.

3.7. Adsorption mechanism

By considering the adsorption of RR 198 onto the surface of PAni/Fe_3O_4, different mechanisms may be involved such as ionic attraction between anionic sulfonate group(s) of dissolved dye molecules and the cationic amino groups of protonated PAni/Fe_3O_4. The possible mechanisms of the adsorption process of PAni/Fe_3O_4 and RR 198 is discussed: In aqueous solution, the RR 198 is first dissolved and the sulphonate groups of RR 198 (D–SO_3Na) is dissociated and converted to anionic dye ions.

$$\mathrm{Dye-SO_3Na} \xrightarrow{\mathrm{H_2O}} \mathrm{Dye-SO_3^-} + \mathrm{Na^+}$$

Also, in the presence of H^+, the amino groups of PAni (–NH_2) are protonated.

$$\mathrm{PAni-NH_2} + \mathrm{H^+} \rightarrow \mathrm{PAni-NH_3^+}$$

Table 5
Calculated different isotherm parameters by linear method

Langmuir isotherm model				Freundlich isotherm model			Temkin isotherm model		
q_m	K_L	R_L	R^2	K_F	n	R^2	K_1	K_2	R^2
45.454	0.128	0.072	0.995	10.350	2.915	0.893	10.12	1.043	0.923

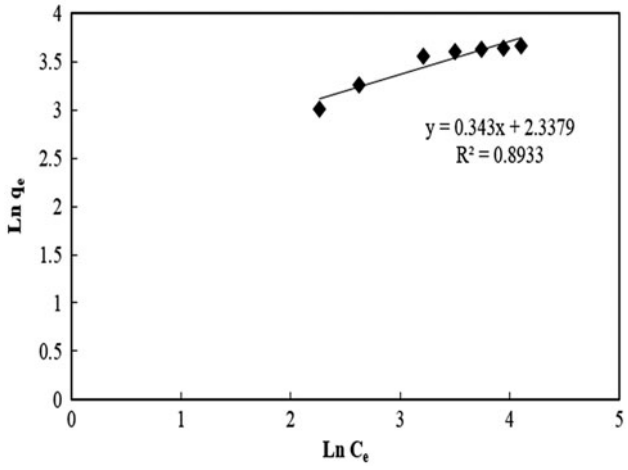

Fig. 13. Removal of dye RR198 with: PAni/Fe_3O_4 (the initial concentration, pH, volume of solution and amount of adsorbent was 70 mg/L, 5, 100 mL, and 0.1 g, respectively), Freundlich isotherm.

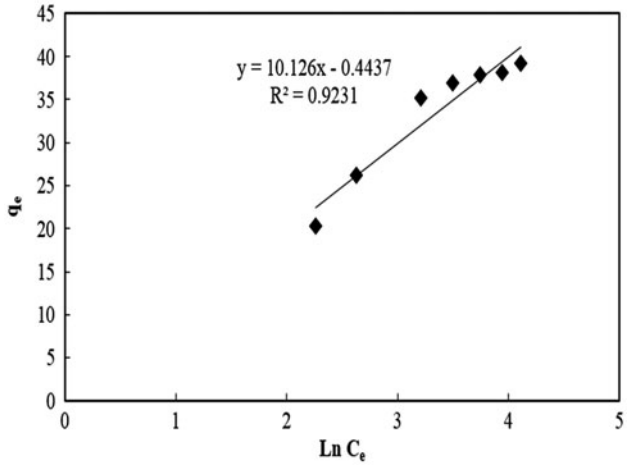

Fig. 14. Removal of dye RR198 with: PAni/Fe_3O_4 (the initial concentration, pH, volume of solution and amount of adsorbent was 70 mg/L, 5, 100 mL, and 0.1 g, respectively), Temkin isotherm.

The adsorption process then proceeds due to the electrostatic attraction between these two counter ions:

$$\mathrm{PAni-NH_3^+ + Dye-SO_3^- \rightarrow PAni-NH_3^+{}_3^-OS - Dye}$$

3.8. Kinetics of adsorption

In this section, for the purpose of investigating the kinetics of the process of RR 198 adsorption on PAni composite, two kinetic models of pseudo-first-order and pseudo-second-order were used.

3.8.1. Pseudo-first-order

A simple kinetic analysis of adsorption is the Lagergren equation, a pseudo-first-order equation describes the kinetics of the adsorption process as follows Eq. (6) [41]:

$$\frac{dq_t}{dt} = k_1(q_e - q_t) \tag{6}$$

where k_1 is the rate constant of pseudo-first-order adsorption (s^{-1}), and q_e and q_t are the amount of dye adsorbed on PAni/Fe_3O_4 (mg/g) at equilibrium and at time t, respectively. After definite integration by applying the initial conditions $q_t = 0$ at $t = 0$ and $q_t = q_t$ at $t = t$, Eq. (7) becomes:

$$\ln(q_e - q_t) = \ln q_e - k_1 t \tag{7}$$

Linear plot feature of $\ln(q_e - q_t)$ against t (Fig. 15) for adsorption of RR 198 on PAni/Fe_3O_4 were achieved and the k_1 and q_e values calculated from slope and intercept of this line were summarized in Table 6.

3.8.2. Pseudo-second-order

The pseudo-second-order rate expression is based on adsorption equilibrium capacity and can be expressed (8) and presented linearly by the following Eq. (9) [41]:

$$\frac{dq_t}{dt} = k_2(q_e - q_t)^2 \tag{8}$$

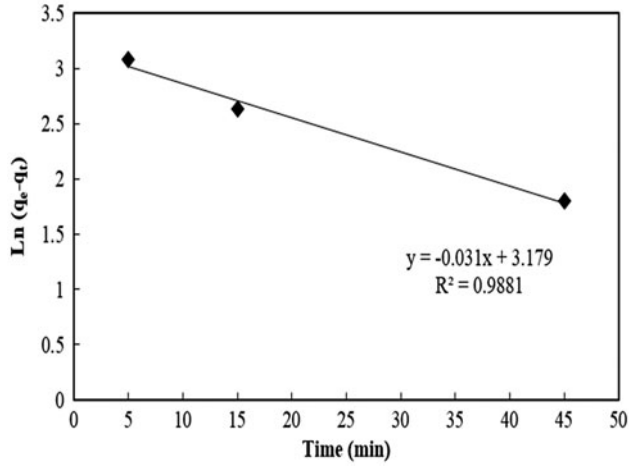

Fig. 15. Removal of dye RR198 with: PAni/Fe_3O_4 (the initial concentration, pH, volume of solution and amount of adsorbent was 70 mg/L, 5, 100 mL, and 0.1 g, respectively), pseudo-first-order.

Table 6
Values of the pseudo-first-order and pseudo-second-order models for adsorption of RR 198 on PAni/Fe_3O_4

	Pseudo-first-order			Pseudo-second-order		
$q_{e,exp}$ (mg/g)	K_1 (min^{-1})	q_e (mg/g)	R^2	K_2 (min^{-1})	q_e (mg/g)	R^2
45.454	0.031	24.022	0.988	0.002	43.478	0.999

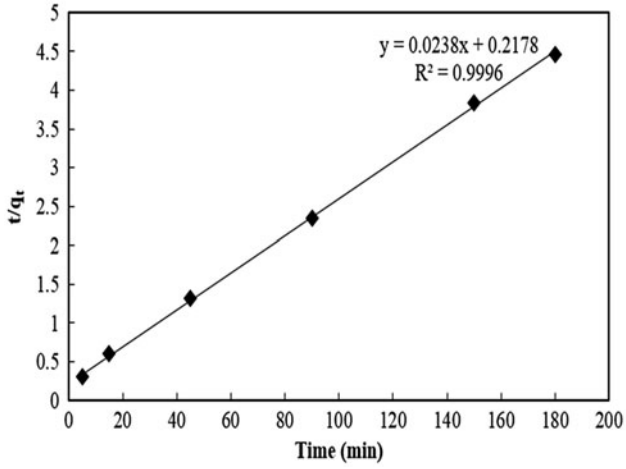

Fig. 16. Removal of dye RR198 with: PAni/Fe_3O_4 (the initial concentration, pH, volume of solution and amount of adsorbent was 70 mg/L, 5, 100 mL, and 0.1 g, respectively), pseudo-second-order.

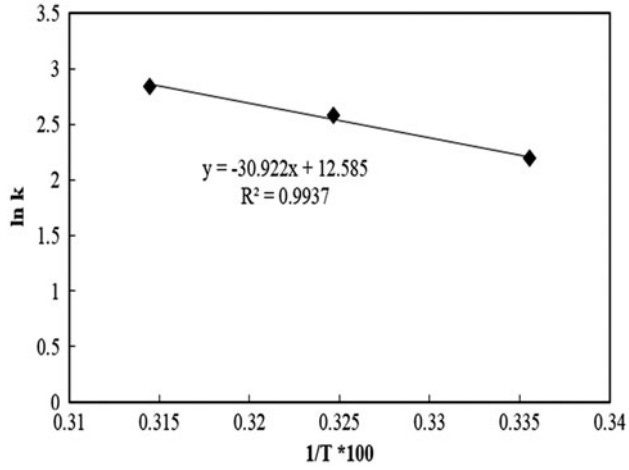

Fig. 17. Removal of dye RR198 with: PAni/Fe_3O_4 (the initial concentration, pH, volume of solution and amount of adsorbent was 70 mg/L, 5, 100 mL, and 0.1 g, respectively), Van't Hoff Regression.

$$\frac{t}{q_t} = \frac{1}{k_2 q_e^2} + \frac{1}{q_e} t \tag{9}$$

In Eq. (8), k_2 is the rate constant of pseudo-second-order adsorption (g/mg min), q_e and q_t are the amount of dye adsorbed on PAni/Fe_3O_4 (mg/g) at equilibrium and at time t, respectively. Linear plot feature of (t/q_t) against t (Fig. 16) for adsorption of RR 198 on PAni/Fe_3O_4 were achieved and the k_2 and q_e values calculated from slope and intercept of this line were summarized in Table 6.

The correlation coefficient (R^2) for both of kinetics models are shown in Table 6. The correlation coefficient of pseudo-second-order is better and higher than pseudo-first-order. Therefore, it can be concluded that the adsorption kinetic of RR 198 on PAni/Fe_3O_4 fitted by pseudo-second-order.

3.9. Gibbs free energy, enthalpy, and entropy

The Gibbs free energy changes (ΔG°) were determined using following Eq. (10):

$$-\Delta G^\circ = RT \ln k \tag{10}$$

where R is the gas constant, T is the absolute temperature (K), and K is the partition ratio. The values of partition ratio (K) and Gibbs free energy change (ΔG°) are presented in Table 7. The negative Values of Gibbs free energy change (ΔG°) confirm that the adsorption of RR 198 onto PAni/Fe_3O_4 is spontaneous and thermodynamically favorable. The more negative values of ΔG° imply that the greater driving force is required for the adsorption process. As the temperature increases, the ΔG° values decrease, indicating less

Table 7
Thermodynamic Parameters (ΔH°, ΔG°, ΔS°) for the Adsorption of RR 198 on PAni/Fe_3O_4

Temperature (℃)	K	ΔG° (kj/mol)	ΔH° (kJ/mol)	ΔS° (J/mol K)	R^2
25	8.974	−5.436	257.068	104.590	0.993
35	13.139	−6.595			
45	17.218	−7.524			

Table 8
A comparison between the results of the present work and some reported results in literature

Sorbent material	Dye	Sorption capacity (mg g^{-1})	Isotherm model	Refs.
Maize Tassel Powder	Reactive Red 198	16.95	Langmuir and Freundlich	[43]
Activated carbon made of walnut wood	Reactive Black 5	14.08	Freundlich	[44]
Agricultural waste	Reactive blue19	12.534	Langmuir	[45]
Azollafiliculoides biomass	Reactive Acid Blue15	7.1	Langmuir	[46]
Bagasse	Reactive blue 4	13.2	Langmuir	[47]
Chitosan microspheres	Reactive Black 5	28.9 ± 2.8	Langmuir	[48]
Wood-shaving bottom ash treated with water (WBA/H_2O)	Reactive Red 141	24.3	Freundlich	[49]
Wood-shaving bottom ash treated with 0.1 N H_2SO_4 (WBA/H_2SO_4)	Reactive Red 141	29.9	Freundlich	[49]
Activated carbon	Reactive Red 141	41.5	Freundlich	[49]
Cotton plant wastes—stalk (CS)	Remazol Black B reactive	35.7	Langmuir, Redlich–Peterson and Langmuir–Freundlich	[50]
PAni/Fe_3O_4 magnetic nanoparticles	Reactive red 198	45.454	Langmuir	This work

driving force and hence resulting in lesser adsorption capacity at higher temperatures.

Standard enthalpy (ΔH°) and entropy (ΔS°) were determined from the Van't Hoff equation [42]:

$$\ln k = \frac{\Delta S^\circ}{R} - \frac{\Delta H^\circ}{RT} \tag{11}$$

ΔH° and ΔS° were obtained from the slope and intercept of the plot of $\ln k$ against $1/T$, as shown in Fig. 17. The values of ΔH° and ΔS° are listed in Table 7. The value of ΔH° is positive, indicating that the adsorption process is endothermic in nature.

4. Conclusion

PAni/Fe_3O_4 magnetic nanoparticle is an effective adsorbent for the removal of Reactive Red 198 dye from water. The maximum removal was observed at a sorbent dose of 0.08 g, contact time of 90 min and pH 5. The equilibrium adsorption was best fitted with the Langmuir isotherm. The maximum dye adsorption capacity of PAni/Fe_3O_4 nano composite obtained from the Langmuir model at 25°C was 45.454 mg g^{-1}. Adsorption kinetics revealed that Reactive Red 198 is well described by a pseudo-second-order model. Based on the results obtained from thermodynamic parameters such as enthalpy change (ΔH°), entropy change (ΔS°), and changes in the Gibbs free energy (ΔG°), it was revealed that the adsorption process was endothermic, feasible and spontaneous. A comparison between the results of the present work and some reported results in the literature is represented in Table 8.

List of symbols

C_0 — initial dye concentration (mg/l)
C_e — equilibrium liquid phase concentration of dye solutions (mg/l)
K_1 — constant related to the heat of adsorption
K_2 — equilibrium binding constant
K_F — Freundlich isotherm constant (mg/g)
K_L — Langmuir isotherm constant (l/mg)
L — liter
n — heterogeneity factor
q_e — amount of dye per gram of sorbent at equilibrium (mg/g)
q_m — Langmuir isotherm constant (mg/g)
q_t — amount of dye adsorbed per gram of sorbent at any time (mg/g)
R — gas constant (8.314 J mol/K)
R_L — dimensionless constant separation factor
R^2 — correlation coefficient
t — time (min)
T — solution temperature (°C, K)
ΔG° — standard free energy change (kJ/mol)
ΔH° — enthalpy change (kJ/mol)
ΔS° — entropy change (kJ/mol)

References

[1] Z. Aksu, Application of biosorption for the removal of organic pollutants: A review, Process Biochem. 40 (2005) 997–1026.

[2] G.M. Walker, L. Hansen, J.A. Hanna, S.J. Allen, Kinetics of a reactive dye adsorption onto dolomitic sorbents, Water Res. 37 (2003) 2081–2089.

[3] M. Doğan, M. Alkan, Adsorption kinetics of methyl violet onto perlite, Chemosphere 50 (2003) 517–528.

[4] D. Inthorn, S. Singhtho, P. Thiravetyan, E. Khan, Decolorization of basic, direct and reactive dyes by pre-treated narrow-leaved cattail (*Typha angustifolia* Linn.), Bioresour. Technol. 94 (2004) 299–306.

[5] W.T. Tsai, C.Y. Chang, M.C. Lin, S.F. Chien, H.F. Sun, M.F. Hsieh, Adsorption of acid dye onto activated carbons prepared from agricultural waste bagasse by $ZnCl_2$ activation, Chemosphere 45 (2001) 51–58.

[6] G. Mezohegyi, A. Kolodkin, U.I. Castro, C. Bengoa, F. Stuber, J. Font, A. Fabregat, A. Fortuny, Effective anaerobic decolorization of azo dye acid orange 7 in continuous upflowpacked-bed reactor using biological activated carbon system, Ind. Eng. Chem. Res. 46 (2007) 6788–6792.

[7] N. Dizge, C. Aydiner, E. Demirbas, M. Kobya, S. Kara, Adsorption of reactive dyes from aqueous solutions by fly ash: Kinetic and equilibrium studies, J. Hazard. Mater. 150 (2008) 737–746.

[8] V.K. Garg, R. Gupta, A. Yadav, K. Kumar, Dye removal from aqueous solution by adsorption on treated sawdust, Bioresour. Technol. 89 (2003) 121–124.

[9] N. Kannan, M. Meenakshisundaram, Adsorption of congo red on various activated carbons, Water Air Soil Pollut. 138 (2002) 289–305.

[10] K. Kadirvelu, M. Palanival, R. Kalpana, S. Rajeswari, Activated carbon from an agricultural by-product, for the treatment of dyeing industry wastewater, Bioresour. Technol. 74 (2000) 263–265.

[11] V.K. Gupta, A. Mittal, L. Krishnan, V. Gajbe, Adsorption kinetics and column operations for the removal and recovery of malachite green from wastewater using bottom ash, Sep. Purif. Technol. 40 (2004) 87–96.

[12] A. Mittal, L. Kurup (Krishnan), V.K. Gupta, Use of waste materials—Bottom Ash and De-Oiled Soya, as potential adsorbents for the removal of Amaranth from aqueous solutions, J. Hazard. Mater. 117 (2005) 171–178.

[13] S. Dadfarnia, M. Talebi, A.M. Haji Shabani, Z. Amani Beni, Determination of lead and cadmium in different samples by flow injection atomic absorption spectrometry incorporating a microcolumn of immobilized ammonium pyrrolidinedithiocarbamate on microcrystalline naphthalene, Croat. Chem. Acta. 80 (2007) 17–23.

[14] A.A. Ensafi, A.R. Ghaderi, On-line solid phase selective separation and preconcentration of Cd(II) by solid-phase extraction using carbon active modified with methyl thymol blue, J. Hazard. Mater. 148 (2007) 319–325.

[15] H. Eisazadeh, Removal of mercury from water using polypyrrole and its composites, Chin. J. Polym. Sci. 25 (2007) 393–397.

[16] H. Eisazadeh, Removal of chromium from waste water using polyaniline, J. Appl. Polym. Sci. 104 (2007) 1964–1967.

[17] X.R. Zeng, T. Man Ko, Structures and properties of chemically reduced polyanilines, Polymer 39 (1998) 1187–1195.

[18] R. Ansari, N. Khoshbakht Fahim, A. Fallah Delavar, Removal of nitrite ions from aqueous solutions using conducting electroactive polymers, Open Process Chem. J. 2 (2009) 1–5.

[19] E.T. Kang, K.G. Neoh, K.L. Tan, Polyaniline, A polymer with many interesting intrinsic redox states, Prog. Polym. Sci. 23 (1998) 277–324.

[20] X.G. Li, A. Li, M.R. Huang, Facile high-yield synthesis of polyaniline nanosticks with intrinsic stability and electrical conductivity, Chem.—A Eur. J. 14 (2008) 10309–10317.

[21] N. Gospodinova, L. Terlemezyan, Conducting polymers prepared by oxidative polymerization: Polyaniline, Prog. Polym. Sci. 23 (1998) 1443–1484.

[22] W.S. Huang, B.D. Humphrey, A.G. MacDiarmid, Polyaniline, a novel conducting polymer. Morphology and chemistry of its oxidation and reduction in aqueous electrolytes, J. Chem. Soc., Faraday Trans. 1: Phys. Chem. Condensed Phases 82 (1986) 2385–2400.

[23] Z. Sabatkova, M. Safarikova, I. Safarik, Magnetic ovalbumin and egg white aggregates as affinity adsorbents for lectins separation, Biochem. Eng. J. 40 (2008) 542–545.

[24] J.S. Becker, O.R.T. Thomas, M. Franzreb, Protein separation with magnetic adsorbents in micellar aqueous two-phase systems, Sep. Purif. Technol. 65 (2009) 46–53.

[25] Z.Y. Ma, Y.P. Guan, H.Z. Liu, Superparamagnetic silica nanoparticles with immobilized metal affinity ligands for protein adsorption, J. Magn. Magn. Mater. 301 (2006) 469–477.

[26] B. Zargar, H. Parham, A. Hatamie, Modified iron oxide nanoparticles as solid phase extractor for spectrophotometeric determination and separation of basic fuchsin, Talanta 77 (2009) 1328–1331.

[27] J.L. Gong, B. Wang, G.M. Zeng, C.P. Yang, C.G. Niu, Q.Y. Niu, W.J. Zhou, Y. Liang, Removal of cationic dyes from aqueous solution using magnetic multi-wall carbon nanotube nanocomposite as adsorbent, J. Hazard. Mater. 164 (2009) 1517–1522.

[28] A. Afkhami, M. Saber-Tehrani, H. Bagheri, Simultaneous removal of heavy metal ions in wastewater samples using nano-alumina modified with 2,4-dinitrophenylhydrazine, J. Hazard. Mater. 181 (2010) 836–844.

[29] A. Afkhami, M. Saber-Tehrani, H. Bagheri, Flame atomic absorption spectrometric determination of trace amounts of Pb(II) andCr(III) in biological, food and environmental samples after preconcentration by modified nano-alumina, Microchim. Acta 172 (2011) 125–136.

[30] C.Z. Huang, B. Hu, Silica-coated magnetic nanoparticles modified with γ- mercaptopropyltrimethoxysilane for fast and selective solid phase extraction of trace amounts of Cd, Cu, Hg, and Pb in environmental and biological samples prior to their determination by inductively coupled plasma mass spectrometry, Spectrochim. Acta, Part B 63 (2008) 437–444.

[31] A. Afkhami, R. Norooz-Asl, Removal, preconcentration and determination of Mo(VI) from water and wastewater samples using maghemite nanoparticles, Colloids Surf. A 346 (2009) 52–57.

[32] A. Afkhami, R. Moosavi, Adsorptive removal of Congo red, a carcinogenic textile dye, from aqueous solutions by maghemite nanoparticles, J. Hazard. Mater. 174 (2010) 398–403.
[33] A. Afkhami, R. Moosavi, T. Madrakian, Preconcentration and spectrophotometric determination of low concentrations of malachite green and leuco-malachite green in water samples by high performance solid phase extraction using maghemite nanoparticles, Talanta 82 (2010) 785–789.
[34] B.R. White, B.T. Stackhouse, J.A. Holcombe, Magnetic γ-Fe_2O_3 nanoparticles coated with poly-l-cysteine for chelation of As(III), Cu(II), Cd(II), Ni(II), Pb(II) and Zn (II), J. Hazard. Mater. 161 (2009) 848–853.
[35] Y.F. Shen, J. Tang, Z.H. Nie, Y.D. Wang, Y. Ren, L. Zuo, Tailoring size and structural distortion of Fe_3O_4 nanoparticles for the purification of contaminated water, Bioresour. Technol. 100 (2009) 4139–4146.
[36] H. Itoh, T. Sugimoto, Systematic control of size, shape, structure, and magnetic properties of uniform magnetite and maghemite particles, J. Colloid Interface Sci. 265 (2003) 283–295.
[37] W. Voit, D.K. Kim, W. Zapka, M. Muhammed, K.V. Rao, Magnetic behavior of coated superparamagnetic iron oxide nanoparticles in ferrofluids, Matter. Res. Soc. 676 (2001) 781–786.
[38] J. Sun, S. Zhou, P. Hou, Y. Yang, J. Weng, X. Li, M. Li, Synthesis and characterization of biocompatible Fe_3O_4 nanoparticles, J. Biomed. Mater. Res. Part A 80A (2007) 333–341.
[39] K. Vasanth Kumar, S. Sivanesan, Isotherm parameters for basic dyes onto activated carbon: Comparison of linear and non-linear method, J. Hazard. Mater. 129 (2006) 147–150.
[40] E.N. El Qada, S.J. Allen, G.M. Walker, Adsorption of Methylene Blue onto activated carbon produced from steam activated bituminous coal: A study of equilibrium adsorption isotherm, Chem. Eng. J. 124 (2006) 103–110.
[41] M. Chairat, S. Rattanaphani, J.B. Bremner, V. Rattanaphani, An adsorption and kinetic study of lac dyeing on silk, Dyes Pigm. 64 (2005) 231–241.
[42] C.I. Bird, W.S. Boston, The Theory of Coloration of Textiles, L. Peters, (Ed.), The Dyers Company Publications Trust, England, 1975.
[43] M. Dehvari, M.T. Ghaneian, F. Fallah, M. Sahraee, B. Jamshidi, Evaluation of maize tassel powder efficiency in removal of reactive red 198 dye from synthetic textile wastewater, J. Community Health Res. 1 (2013) 153–165.
[44] A.H. Mahvi, B. Heibati, A.R. Yari, N. Vaezi, Efficiency of reactive black 5 dye removals and determination of isotherm models in aqueous solution by use of activated carbon made of walnut wood, Res. J. Chem. Environ. 16 (2012) 26–30.
[45] M. Abassi, N. Razzaghi Asl, Removal of hazardous reactive blue19 dye from aqueous solutions by agricultural waste, J. Iran. Chem. Res. 2 (2009) 221–230.
[46] M.A. Zazouli1, D. Balarak, Y. Mahdavi, F. Karimnejad, The application of Azollafiliculoides biomass in acid blue 15 dye (AB15) removal from aqueous solutions, J. Bas Res. Med. Sci. 1 (2014) 29–37.
[47] A.E.A.A. Said, A.A. Aly, M.M.A. El-Wahab, S.A. Soliman, A.A.A. El-Hafez, V. Helmey, M.N. Goda, Application of modified bagasse as a biosorbent for reactive dyes removal from industrial wastewater, J. Water Resour. Protect., 5 (2013) 10–17.
[48] I.Y. Kimura1, V.T. Fávere, A.O. Martins, V.A. Spinelli, A. Josué, Adequacy of isotherm adsorption of black 5 reactive dye for crosslinked chitosan microspheres, Acta Sci.Technol. 23 (2001) 1313–1317.
[49] P. Leechart, W. Nakbanpote, P. Thiravetyan, Application of 'waste' wood-shaving bottom ash for adsorption of azo reactive dye, J. Environ. Manage. 90 (2009) 912–920.
[50] Ö. Tunç, H. Tanacı, Z. Aksu, Potential use of cotton plant wastes for the removal of Remazol Black B reactive dye, J. Hazard. Mater. 163 (2009) 187–198.